Anomalous gauge couplings of the Higgs boson at the CERN LHC: Semileptonic mode in WW scatterings

Yong-Hui Qi,[1,2] Yu-Ping Kuang,[1,2] Bei-Jiang Liu,[3] and Bin Zhang[1,2]
[1]*Department of Physics, Tsinghua University, Beijing, 100084, China*
[2]*Center for High Energy Physics, Tsinghua University, Beijing, 100084, China*
[3]*Institute of High Energy Physics, Academia Sinica, Beijing, 100039, China*
(Received 21 November 2008; published 16 March 2009)

We make a full tree level study of the signatures of anomalous gauge couplings of the Higgs boson at the CERN LHC via the semileptonic decay mode in WW scatterings, $pp \to W^+W^\pm j_1^f j_2^f \to l^+\nu_l j_1 j_2 j_1^f j_2^f$. Both signals and backgrounds are studied at the hadron level for the Higgs mass in the range 115 GeV $\leq m_H \leq$ 200 GeV. We carefully impose suitable kinematical cuts for suppressing the backgrounds. To the same sensitivity as in the pure leptonic mode $pp \to W^+W^+ j_1^f j_2^f \to l^+\nu_l l^+\nu_l j_1^f j_2^f$, our result shows that the semileptonic mode can reduce the required integrated luminosity by a factor of 3. If the anomalous couplings in nature are actually larger than the sensitivity bounds shown in the text, the experiment can start the test for an integrated luminosity of 50 fb^{-1}.

DOI: 10.1103/PhysRevD.79.055010 PACS numbers: 12.60.Fr, 11.15.Ex, 14.80.Cp

I. INTRODUCTION

Although the standard model (SM) has passed all the LEP electroweak precision tests, its spontaneous symmetry breaking sector is still a puzzle. The Higgs boson has not been found yet. The LEP direct search bound on the SM Higgs mass is $m_H > 114.4$ GeV [1], and the 95% CL upper bound on m_H from the LEP precision data is $m_H \leq$ 167 GeV [1]. This range of the SM Higgs mass is within the coverage of the CERN Large Hadron Collider (LHC), and searching for the Higgs boson is of first priority in LHC experiments. Theoretically, the SM Higgs sector suffers from the well-known problems of *triviality* [2] and *unnaturalness* [3]. Therefore, there must be a scale of new physics, Λ, above which the SM should be replaced by certain new physics model. Naturalness implies that $\Lambda \sim O$ (TeV). Direct search for the new heavy particle(s) with mass $M \geq \Lambda$ at the LHC may or may not be easy depending on how high Λ actually is and their properties. However, they will affect the couplings between lighter particles through virtual processes. Once a light Higgs boson candidate is found at the LHC, the first question to be answered is whether it is the SM Higgs boson or a Higgs boson in certain new physics model. The contribution of new heavy particles to the couplings related to the Higgs boson will cause the couplings anomalous (different from the SM values), therefore measuring the anomalous Higgs couplings can answer the above question. The anomalous couplings of the Higgs boson to electroweak (EW) gauge bosons are of special interest since they are related to the mass generation mechanism of the W and Z bosons. In this paper, we concentrate on studying sensitive processes for measuring those anomalous coupling constants at the LHC.

Since we do not know what the new physics model above Λ really is, we study it in a general model independent way. There have been various formulations describing the effective anomalous couplings between the Higgs boson and the EW gauge bosons, namely, the linear realization formulation [4–6] and the nonlinear realization formulation [7]. In this paper, we take the popular linear realization formulation given in [4,6] to perform the study. In this formulation, the main anomalous gauge couplings of the Higgs boson deviating from the SM coupling are of dimension six. The CP conserving effective Lagrangian for the anomalous interactions is formulated as [4,6]

$$\mathcal{L}_{\text{eff}} = \sum_n \frac{f_n}{\Lambda^2}\mathcal{O}_n, \tag{1}$$

where f_n's are dimensionless *anomalous couplings*. In the SM, $f_n = 0$. The gauge-invariant dimension-six operators $\mathcal{O}_n$'s are [6]

$$\begin{aligned}
\mathcal{O}_{BW} &= \Phi^\dagger \hat{B}_{\mu\nu}\hat{W}^{\mu\nu}\Phi,\\
\mathcal{O}_{DW} &= \mathrm{Tr}([D_\mu, \hat{W}_{\nu\rho}], [D^\mu, \hat{W}^{\nu\rho}]),\\
\mathcal{O}_{DB} &= -\frac{g'^2}{2}(\partial_\mu B_{\nu\rho})(\partial^\mu B^{\nu\rho}),\\
\mathcal{O}_{\Phi,1} &= (D_\mu\Phi)^\dagger\Phi^\dagger\Phi(D^\mu\Phi),\\
\mathcal{O}_{\Phi,2} &= \frac{1}{2}\partial^\mu(\Phi^\dagger\Phi)\partial_\mu(\Phi^\dagger\Phi),\\
\mathcal{O}_{\Phi,3} &= \frac{1}{3}(\Phi^\dagger\Phi)^3,\\
\mathcal{O}_{WWW} &= \mathrm{Tr}[\hat{W}_{\mu\nu}\hat{W}^{\nu\rho}\hat{W}^\mu_\rho],\\
\mathcal{O}_{WW} &= \Phi^\dagger\hat{W}_{\mu\nu}\hat{W}^{\mu\nu}\Phi,\\
\mathcal{O}_{BB} &= \Phi^\dagger\hat{B}_{\mu\nu}\hat{B}^{\mu\nu}\Phi,\\
\mathcal{O}_W &= (D_\mu\Phi)^\dagger\hat{W}^{\mu\nu}(D_\nu\Phi),\\
\mathcal{O}_B &= (D_\mu\Phi)^\dagger\hat{B}^{\mu\nu}(D_\nu\Phi),
\end{aligned} \tag{2}$$

where $\hat{B}_{\mu\nu}$ and $\hat{W}_{\mu\nu}$ stand for

$$\hat{B}_{\mu\nu} = i\frac{g'}{2}B_{\mu\nu}, \qquad \hat{W}_{\mu\nu} = i\frac{g}{2}\sigma^a W^a_{\mu\nu}, \tag{3}$$

in which g and g' are the $SU(2)$ and $U(1)$ gauge coupling constants, respectively.

It has been shown that the operators $O_{\Phi,1}$, O_{BW}, O_{DW}, O_{DB} are related to the two-point functions of the weak bosons, so that they are severely constrained by the precision EW data [6]. For example, O_{BW} and $O_{\Phi,1}$ are related to the oblique correction parameter S and T, and are thus strongly constrained by the precision EW data. The 2σ constraints on $|f_{BW}/\Lambda^2|$ and $|f_{\Phi,1}/\Lambda^2|$ are $|f_{BW}/\Lambda^2|$, $|f_{\Phi,1}/\Lambda^2| < O(10^{-2})$ TeV^{-2} [8]. The operators $O_{\Phi,2}$ and $O_{\Phi,3}$ are related to the triple and quartic Higgs boson self-interactions, and have been studied in detail in Ref. [9]. The operator O_{WWW} is related to the weak boson self-couplings, so that it is irrelevant to the present study. The precision and low energy EW data are not sensitive to the remaining four operators O_{WW}, O_{BB}, O_W, and O_B. These four anomalous couplings are only constrained by the requirement of the unitarity of the S matrix, and such theoretical constraints are quite weak [10]. For example, the unitarity constraints on f_W/Λ^2 and f_{WW}/Λ^2 are [8,10]

$$\left|\frac{f_W}{\Lambda^2}\right| \le 7.8 \text{ TeV}^{-2}, \qquad \left|\frac{f_{WW}}{\Lambda^2}\right| \le 39.2 \text{ TeV}^{-2}. \tag{4}$$

The test of these four anomalous Higgs couplings at the LHC is what we shall concentrate on. The sensitivity of the test is crucial for discriminating models.

Taking account of the mixing in the neutral gauge boson sector, the effective Lagrangian expressed in terms of the photon field A_μ, the weak boson fields $W^\pm_\mu$, Z_μ, and the Higgs boson field H is [6]

$$\begin{aligned}\mathcal{L}^H_{\text{eff}} &= g_{H\gamma\gamma}HA_{\mu\nu}A^{\mu\nu} + g^{(1)}_{HZ\gamma}A_{\mu\nu}Z^\mu\partial^\nu H \\ &\quad + g^{(2)}_{HZ\gamma}HA_{\mu\nu}Z^{\mu\nu} + g^{(1)}_{HZZ}Z_{\mu\nu}Z^\mu\partial^\nu H \\ &\quad + g^{(2)}_{HZZ}HZ_{\mu\nu}Z^{\mu\nu} + g^{(1)}_{HWW}(W^+_{\mu\nu}W^{-\mu}\partial^\nu H \\ &\quad + \text{H.c.}) + g^{(2)}_{HWW}HW^+_{\mu\nu}W^{-\mu\nu},\end{aligned} \tag{5}$$

where the anomalous couplings $g^{(i)}_{HVV}$ with $i = 1, 2$ (V_μ stand for A_μ, $W^\pm_\mu$ or Z_μ) are related to the anomalous couplings f_n's by

$$\begin{aligned} g_{H\gamma\gamma} &= -\kappa\frac{s^2(f_{BB}+f_{WW})}{2}, & g^{(1)}_{HZ\gamma} &= \kappa\frac{s(f_W-f_B)}{2c}, \\ g^{(2)}_{HZ\gamma} &= \kappa\frac{s[s^2f_{BB}-c^2f_{WW}]}{c}, & g^{(1)}_{HZZ} &= \kappa\frac{c^2f_W+s^2f_B}{2c^2}, \\ g^{(2)}_{HZZ} &= -\kappa\frac{s^4f_{BB}+c^4f_{WW}}{2c^2}, & g^{(1)}_{HWW} &= \kappa\frac{f_W}{2}, \\ g^{(2)}_{HWW} &= -\kappa f_{WW}, \end{aligned} \tag{6}$$

in which $s \equiv \sin\theta_W$, $c \equiv \cos\theta_W$, and $\kappa \equiv \frac{gM_W}{\Lambda^2} \approx 0.053(\frac{1 \text{ TeV}}{\Lambda})^2$ TeV^{-1}.

Once nonvanishing values of these anomalous couplings (after subtracting the corresponding SM loop corrections) are detected experimentally, it implies that we have already seen the effect of new physics beyond the SM. There have been papers studying the test of the above four anomalous Higgs couplings at the LHC [8,11,12], the linear collider [9,13], and the photon colliders [14]. So far the most sensitive test at the LHC is via the pure leptonic mode in W^+W^+ scattering, $pp \to W^+W^+j^f_1j^f_2 \to l^+\nu_l l^+\nu_l j^f_1 j^f_2$ ($j^f_1j^f_2$ are the two forward jets characterizing WW fusion). This process is sensitive in testing the anomalous couplings f_W and f_{WW} but less sensitive in testing f_B and f_{BB} [8]. The obtained 3σ constraints for an integrated luminosity of 300 fb^{-1} on f_W and f_{WW} are [8]

$$\frac{|f_W|}{\Lambda^2} \le 1.6 \text{ TeV}^{-2}, \qquad \frac{|f_{WW}|}{\Lambda^2} \le 2.9 \text{ TeV}^{-2}. \tag{7}$$

We see that these values are significantly smaller than the unitarity bounds (4), so that there is plenty of room for detectable f_W/Λ^2 and f_{WW}/Λ^2 within the unitarity bounds.

However, the required integrated luminosity 300 fb^{-1} is rather high. The LHC needs several years after its first collision to reach this high integrated luminosity. In this paper, we study the possibility of taking the semileptonic mode, which can have a larger cross section. Since it is not possible to distinguish $W^+ \to j_1j_2$ and $W^- \to j_1j_2$ experimentally, we have to study the scatterings $pp \to W^+W^\pm j^f_1j^f_2$ with $W^+ \to l^+\nu_l$, $W^\pm \to j_1j_2$. There are four jets in the final state, so that the study of the signal and backgrounds is much more complicated than that in the pure leptonic mode. We have to calculate at the hadron level rather than the parton level. We shall show that, from a detailed study, certain kinematic cuts can suppress the backgrounds, and the required integrated luminosity for reaching the 3σ sensitivity (7) can be reduced to 100 fb^{-1}. If the anomalous couplings in the real world are not so small, say larger than the 1σ bounds $-3.5 \text{ TeV}^{-2} \le f_W/\Lambda^2 \le 1.3 \text{ TeV}^{-2}$ or $-0.9 \text{ TeV}^{-2} \le f_{WW}/\Lambda^2 \le 0.8 \text{ TeV}^{-2}$, the LHC can already detect their effect when the integrated luminosity reaches 50 fb^{-1}. If they are larger than the bounds $-4.5 \text{ TeV}^{-2} \le f_W/\Lambda^2 \le 2.4 \text{ TeV}^{-2}$ or $-2.0 \text{ TeV}^{-2} \le f_{WW}/\Lambda^2 \le 1.5 \text{ TeV}^{-2}$, a 3σ detection can be performed at the LHC for an integrated luminosity of 50 fb^{-1}.

This paper is organized as follows. In Sec. II, we briefly sketch some key points in the calculation of weak boson scatterings at the LHC. All the main backgrounds and kinematic cuts for suppressing the backgrounds are investigated in Sec. III. The numerical results of the cross sections and detecting sensitivities under the imposed kinematic cuts are presented in Sec. IV. Section V is a concluding remark.

II. WEAK BOSON SCATTERINGS

Weak boson scatterings ($VV \to VV$) at the LHC are usually regarded as useful processes for probing strongly interacting electroweak symmetry breaking (EWSB) mechanism, and have been studied in detail [15]. In addition, even if EWSB is driven by light Higgs boson, it has been shown that $VV \to VV$ also provide sensitive tests of the anomalous gauge couplings of the Higgs boson [8]. Some anomalous gauge couplings of the Higgs boson may be first detected in on-shell Higgs productions to a lower sensitivity [12]. Weak boson scatterings can then provide further sensitive tests to get more useful information about new physics.

In weak boson scatterings (cf. Fig. 1(a)), a quark q_1 in a proton becomes a forward jet j_1^f (from the outgoing quark q_1') after emitting a weak boson. It can be seen from helicity analysis that, if j_1^f and j_2^f are sufficiently forward, the emitted weak bosons are mainly longitudinal. So that the "initial state" weak bosons in Fig. 1 are V_L's. Let us look at the longitudinal weak boson scatterings $V_L V_L \to V_L V_L$. At tree level, there are two kinds of weak boson scattering amplitudes shown in Fig. 1(b), namely, the amplitude containing only gauge bosons $T(V)$, and the amplitude containing Higgs boson exchanges $T(H)$. Since the longitudinal polarization vector depends on the momentum of V_L, the two amplitudes $T(V)$ and $T(H)$ all depend on the center of mass energy E as E^2. In the SM, the coupling constant between the Higgs boson and weak bosons in $T(H)$ is the same as the gauge coupling constant g in $T(V)$. This makes the E^2-dependence terms in $T(V)$ and $T(H)$ exactly cancel in the total amplitude $T(V) + T(H)$, leading to a E^0 dependence of the total amplitude, which guarantees the unitarity of the S matrix. In the case that the HVV couplings in $T(H)$ are anomalous, the cancellation will not be exact, which leads to a E^2 dependence of the total amplitude. The magnitude of the remained E^2 dependence depends on the size of the anomalous couplings. So far as the anomalous couplings are within the untarity bounds (4), there is no violation of the unitarity of the S matrix below the new physics scale Λ. Thus, in the high energy region of the LHC, the cross section is quite different from that in the SM. This is the reason why weak boson scatterings provide sensitive tests of the anomalous couplings. Different from the case of testing the strongly interacting EWSB mechanism in Ref. [15], the signal in the present case is defined as the cross section with anomalous couplings $f_n \neq 0$ rather than the longitudinal cross section. So the $V_L V_L \to V_L V_T, V_T V_T$ contributions with $f_n \neq 0$ are also signals. However, the transverse polarization vector is not momentum dependent, so that the $V_L V_L \to V_L V_L$ contribution with $f_n \neq 0$ is the most sensitive signal.

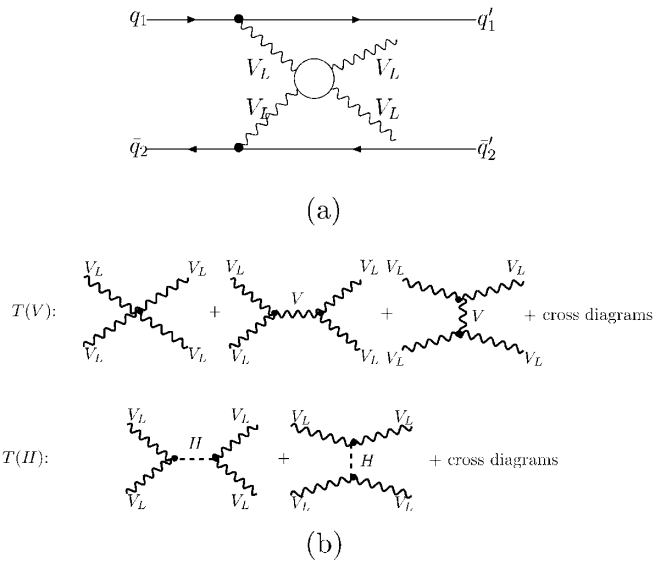

FIG. 1. (a) symbolic diagrams for weak boson scatterings. (b) the two kinds of scattering amplitudes $T(V)$ and $T(H)$ in weak boson scatterings.

At the parton level, the signals and backgrounds in the gold-plated pure leptonic modes of weak boson scatterings have been studied systematically in Ref. [15]. Studying at the parton level, Ref. [8] showed that the $W_L^+ W_L^+ \to W_L^+ W_L^+$ process is the most sensitive one for testing the anomalous couplings (6). Now we are going to study the semileptonic mode with $W^+ W^+ \to l^+ \nu_l j_1 j_2$. Since it is not possible to distinguish the jets from $W_L^+ \to j_1 j_2$ and $W_L^- \to j_1 j_2$ experimentally, we have to take account of both the $W_L^+ W_L^+$ and $W_L^+ W_L^-$ productions and tag the final state $W_L^+ W_L^\pm \to l^+ \nu_l j_1 j_2$. So we are going to calculate the full tree level contributions to the process

$$pp \to W^+ W^\pm j_1^f j_2^f \to l^+ \nu_l j_1 j_2 j_1^f j_2^f, \tag{8}$$

where W^+ and $W^\pm$ are on shell. Now the final state contains four jets, namely, the two forward jets $j_1^f j_2^f$ and the two jets $j_1 j_2$ from $W^\pm$ decays, so that the parton level study is not sufficient for finding out the suitable kinematic cuts to suppress the large backgrounds.

In the following, we shall work at the hadron level, calculating the full tree level contributions to the signal and backgrounds using the helicity amplitude methods [16] and the package PYTHIA [17] with its default fragmentation model. For the parton distribution functions, we take CTEQ6L [18]. For the reconstruction of the W boson from the two jets $j_1 j_2$, we take the cluster-type jet algorithm [19], and using the package ALPGEN [20]. We shall develop suitable kinematic cuts to suppress the backgrounds and save the signal as much as possible.

The backgrounds to $V_L V_L$ scatterings can be classified into three kinds, namely, the EW background, the QCD background, and the top quark background [15]. The irreducible EW background amplitudes (with the same final state particles as the signal) should be calculated together with the signal amplitude to guarantee gauge invariance.

Other backgrounds with different initial or final state particles can be calculated separately.

Let $\sigma(f_n \neq 0)$ and $\sigma_B \equiv \sigma(f_n = 0)$ be the total and background cross sections, respectively. We define the signal cross section σ_S by

$$\sigma_S \equiv \sigma(f_n \neq 0) - \sigma_B. \tag{9}$$

Now the main experimental interest is to find out new physics effect beyond the SM background. Let N_S and N_B be the numbers of the signal events and background events, respectively. For large values of N_S and N_B, we determine the statistical significance σ_{stat} according to

$$\sigma_{\text{stat}} = \frac{N_S}{\sqrt{N_B}}. \tag{10}$$

However, the simple expression (10) holds only when N_S and N_B are large. For general values of N_S and N_B, (10) is not precise enough, and we should take the general Poisson probability distribution approach

$$P_B = \sum_N e^{-N_B} \frac{N_B^N}{N!}, \qquad N = N_S + N_B, N_S + N_B + 1, \cdots, \infty. \tag{11}$$

From the obtained value of $1 - P_B$, we can find out the corresponding value of σ_{stat} [1]. The value of σ_{stat} obtained in this way approaches to that given in (10) when N_S and N_B are sufficiently large. We shall take the approach (11) throughout this paper.

III. BACKGROUNDS AND CUTS

Now we consider all the three kinds of backgrounds to $pp \to W^+W^\pm j_1^f j_2^f \to l^+\nu_l j_1 j_2 j_1^f j_2^f$, and study suitable kinematic cuts for suppressing them.

Considering the actual acceptance of the detectors at the LHC, we always require all the final state particles to be in the following rapidity range throughout this paper

$$|\eta| < 4.5. \tag{12}$$

Recently, Ref. [21] provided a systematic hadron level study of the semileptonic modes in WW scatterings at the LHC for testing the EW chiral Lagrangian coefficients when there are heavy resonances enhancing the scattering cross section at high energies. Although we assume there is no heavy resonances in our present case, the cross section is also enhanced at high energies by the energy dependence arising from the anomalous couplings. Thus, the new techniques developed in Ref. [21] are also useful in our case. We shall apply some of their techniques to our study of testing the anomalous couplings of the light Higgs boson.

A. Signal and irreducible backgrounds

As mentioned above that the signal and irreducible background amplitudes should be put together in the calculation to guarantee gauge invariance. Take the $pp \to W^+W^+J_1^f j_2^f$ process as an example. The typical Feynman diagrams for these amplitudes are shown in Fig. 2 in which Fig. 2(b) (containing Higgs boson exchange) is the signal, and the total contribution of these diagrams with $f_n = 0$ is the irreducible backgrounds.

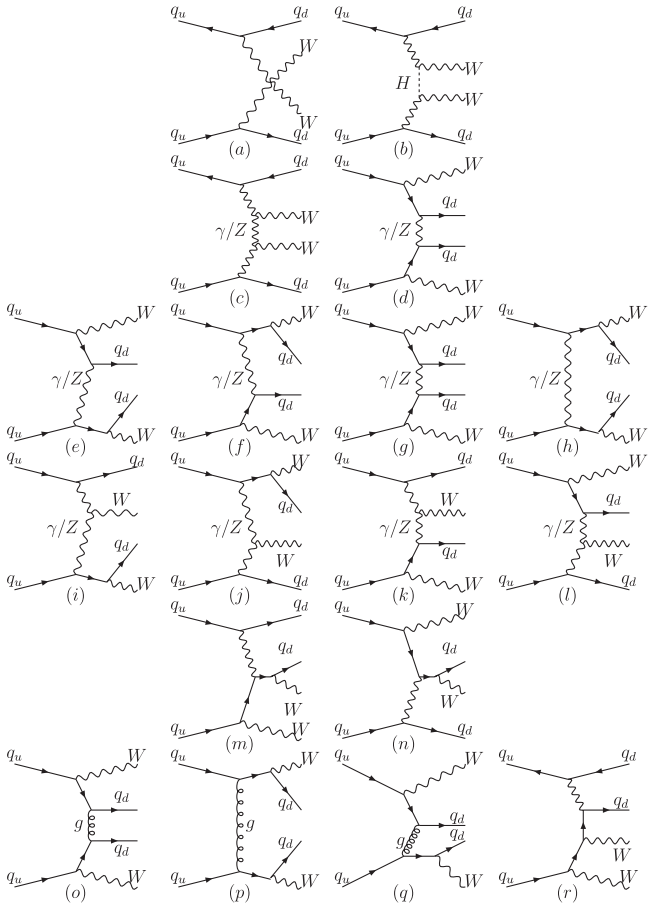

FIG. 2. Typical Feynman diagrams for the signal and irreducible backgrounds in W^+W^+ scattering.

The final state particles in the signal process contains two forward jets $j_1^f j_2^f$, two jets $j_1 j_2$ from $W^\pm$ decays, a positively charged lepton l^+, and a missing neutrino ν_l. Let us consider the cuts for each of the final state particles for extracting the signal.

1. Charged lepton and forward jets

Let us first consider the cut for the transverse momentum of the charged lepton l^+. Since the W^+ boson is quite energetic, the charged lepton l^+ moves almost along the direction of W^+. So we can look at the transverse momentum distribution of W^+. Take the case of f_{WW} dominant as an example. Fig. 3 shows the transverse momentum distributions of the W^+ decaying into leptons with $f_{WW}/\Lambda^2 = 4\ \text{TeV}^{-2}$, $f_W/\Lambda^2 = 0$, and with $f_{WW}/\Lambda^2 = f_W/\Lambda^2 = 0$ (the irreducible background), respectively.

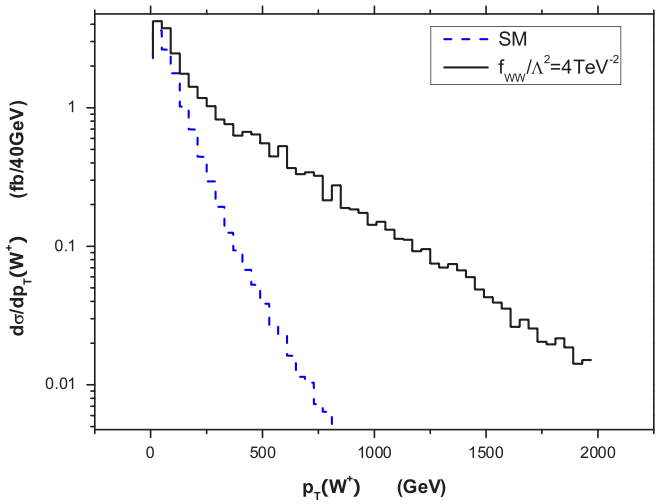

FIG. 3 (color online). $d\sigma/dp_T(W^+)$ distributions: The solid and dashed curves stand for the cases of $f_{WW}/\Lambda^2 = 4$ TeV^{-2}, $f_W/\Lambda^2 = 0$ and $f_{WW}/\Lambda^2 = f_W/\Lambda^2 = 0$, respectively.

We see that the distribution including the signal is significantly harder than that of the irreducible background. Thus, we know that the transverse momentum distribution of the signal l^+ is significantly harder than that of the background l^+. From Fig. 3, we see that imposing the following $p_T(l^+)$ cut can suppress the irreducible background and keep the signal as much as possible,

$$p_T(l^+) > 200 \text{ GeV}. \tag{13}$$

After the cut (13), the jets in most of the irreducible background processes are mainly in the low $|\eta|$ region. Thus, imposing the requirement of the forward jets will effectively suppress this background. The observation of the tagging forward jets do not depend on whether we are testing the strongly interacting EWSB mechanism or testing the anomalous couplings of a light Higgs boson. So we can follow Ref. [21] to impose the following cuts on the transverse momentum $p_T(j^f)$, the energy $E(j^f)$, and the pseudorapidity $\eta(j^f)$ of the two tagging forward jets [21]

$$\begin{aligned} &p_T(j_i^f) > 20 \text{ GeV}, \qquad E(j_i^f) > 300 \text{ GeV}, \\ &2.0 < |\eta(j_i^f)| < 4.5, \qquad i = 1, 2, \\ &\eta(j_1^f)\eta(j_2^f) < 0. \end{aligned} \tag{14}$$

The rapidity cuts in (14) guarantee the two forward jets moving almost back to back. Later, we shall see that this forward jet cut will also suppress the W + jets QCD background and the top quark background effectively. The efficiency of these cuts are listed in the second and third rows in Table I. We see that the cuts (13) and (14) can suppress the irreducible background quite effectively.

2. Hadronic decay of the W boson

Now we come to the issue of extracting the $W^\pm \to j_1 j_2$ events. Since the final state $W^\pm$ is very energetic, 98% of the two jets $j_1 j_2$ behave like a "single" energetic jet J along the $W^\pm$ direction [21], we first use the k_T algorithm (the ALPGEN package [20]) with E combination to pick up the most energetic "single jet." Since $W^\pm$ and W^+ are almost back to back, we can impose the following cuts:

$$p_T(J) > 200 \text{ GeV}, \qquad \eta(J)\eta(l^+) < 0, \tag{15}$$

and requiring the invariant mass M_J to reconstruct the $W^\pm$ mass, i.e.,

$$65 \text{ GeV} < M_J < 95 \text{ GeV}, \tag{16}$$

in which we have considered the realistic detection resolution ± 15 GeV [22].

B. QCD backgrounds

One of the important QCD backgrounds is the $pp \to W + \hat{n}$ partons, which may lead to the final state $W + n$ jets at the hadron level. The case that three of the n jets are detected (with other jets undetected), will be a background to the signal. We have examined the cases for $\hat{n} = 1, 2, 3, 4$ and found that the most important background comes from $\hat{n} = 2$. Thus, the main QCD background of this kind is

TABLE I. Cut efficiency of the cross sections (in fb) for the signal with irreducible background (IB) and other backgrounds with the Higgs boson mass $m_H = 115$ GeV, and the anomalous coupling $f_W/\Lambda^2 = 4.0$ TeV^{-2} (with other anomalous couplings vanishing) as an example.

Cuts	Signal with IB	IB ($f_W = 0$)	WZ + 2-jet	W + 3-jet	$t\bar{t}$
Without cuts	210.66	338.82	1431.67	2908923	407776.84
Equation (13)	34.55	36.08	36.93	9630.86	2586.47
Equation (14)	11.29	9.44	2.40	104.25	61.77
Equations (15) and (16)	7.01	4.12	0.12	0.10	1.09
Equation (19)	2.42	1.29	2.7×10^{-2}	6.1×10^{-3}	0.09
Equation (20) and top quark veto	2.39	1.27	2.3×10^{-2}	4.7×10^{-3}	0.06
Equation (21)	2.28	1.26	5×10^{-4}	2×10^{-4}	2×10^{-3}
Minijet veto	2.28	1.26	-	-	-

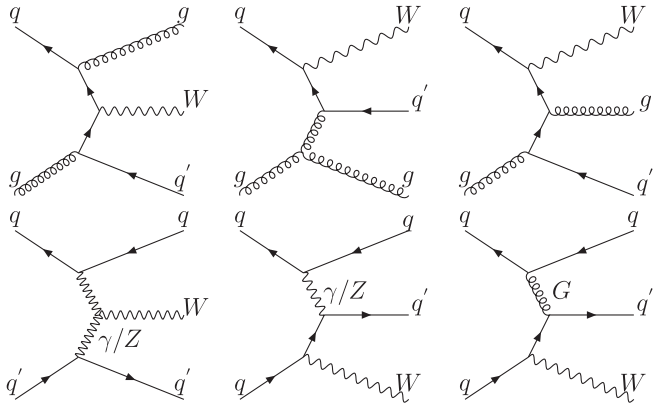

FIG. 4. Typical diagrams for W + 2-parton.

$$pp \to W + \text{2-parton} \to W + \text{3-jet}. \tag{17}$$

The typical Feynman diagrams for qq, $qg \to W +$ 2-parton are depicted in Fig. 4.

Another similar QCD background is

$$q\bar{q}, qg, gg \to WW + n\text{-jet}. \tag{18}$$

As mentioned above, the jets in the backgrounds (17) and (18) are less forward than the forward jets in the signal process when the lepton l^+ is constrained by (13). So imposing the cuts (13) and (14) can suppress these two kinds of QCD backgrounds effectively. Furthermore, the requirements (15) and (16) can significantly suppress this kind of background.

We can further impose a cut to suppress the above QCD backgrounds. The y cut method (imposing a cut on $\log(p_T\sqrt{y})$) developed in Ref. [21] is very effective for this purpose. Fig. 5 shows the $\log(p_T\sqrt{y})$ distributions for

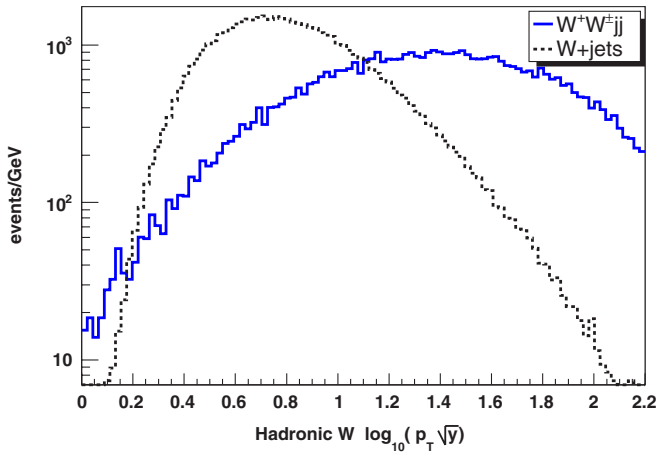

FIG. 5 (color online). $\log(p_T\sqrt{y})$ distributions for the $pp \to W^+W^\pm j_1^f j_2^f$ and $pp \to W +$ 3-jet processes with $f_W/\Lambda^2 = 4\ \text{TeV}^{-2}$, $f_W/\Lambda^2 = 0$.

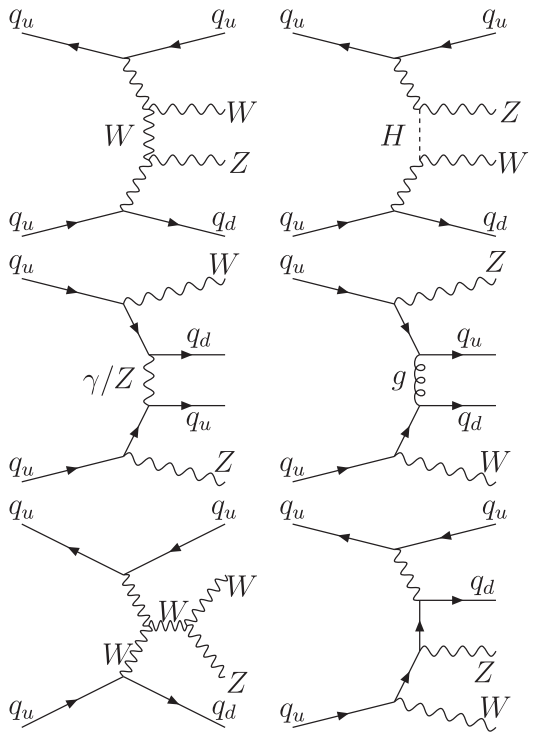

FIG. 6. Typical diagrams for the WZ + 2-jet background.

the $pp \to W^+W^\pm j_1^f j_2^f$ (with $f_W/\Lambda^2 = 4\ \text{GeV}^{-2}$) and $pp \to W +$ 3-jet processes.

From Fig. 5 we see that a cut [21]

$$1.6 < \log(p_T\sqrt{y}) < 2.0 \tag{19}$$

can effectively suppress the backgrounds. Indeed, after the cut (15), (16), and (19), the above QCD backgrounds are significantly reduced (cf. the fourth and fifth rows in Table I).

There is also a kind of important QCD background, which is the $WZjj$ process (cf. Fig. 6) since M_Z is within the range in (16). This includes the WZ scattering process, $pp \to W^+Zj_1^f j_2^f$, which is quite similar to the signal process $pp \to W^+W^\pm j_1^f j_2^f$. However, M_Z is close to the upper bound in (16), i.e., a large portion of the tail of the M_Z resonance higher than the peak is cut away by (16), so that the WZ scattering background is significantly smaller than the signal. However, there are processes of this kind other than WZ scattering (cf. Fig. 6), which can be large. We see from the fourth column of Table I that all the cuts imposed above can effectively suppress this kind of background.

Figure 7 shows the reconstructed W boson peak in the signal process and the Z boson peak in the WZ scattering background after imposing the above cuts. We see that the W boson peak is clearly reconstructed, and the Z boson peak is significantly suppressed by the condition (16).

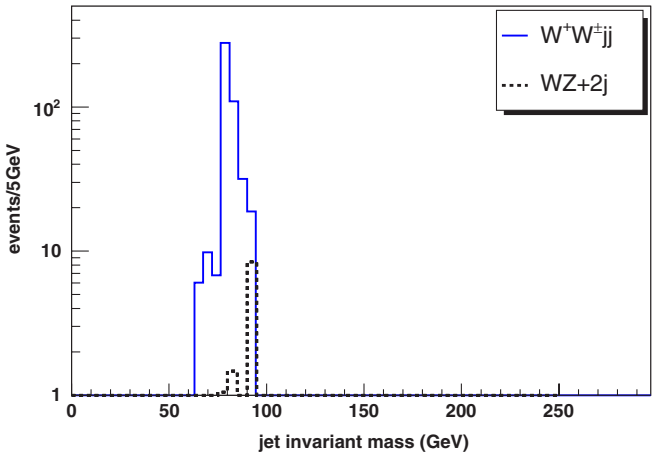

FIG. 7 (color online). Reconstruction of the $W^{\pm}$ boson after the cuts (15) and (16). The solid curve is the $W^{\pm}$ peak in the signal process; the dashed curve shows the Z boson peak in the $WZ + 2$-jet background.

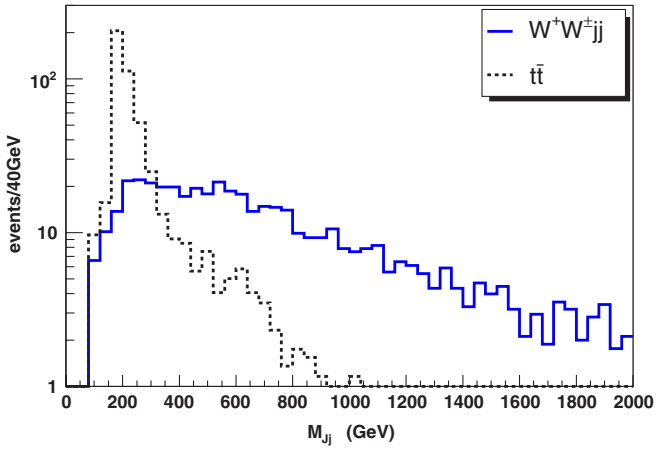

FIG. 9 (color online). Invariant mass M_{Jj} distributions for the top quark background (dashed curve) and the $pp \to W^+W^{\pm} j_1^f j_2^f$ process (solid curve).

C. Top quark background

W boson productions from the decay of top quarks in $t\bar{t}$ production (cf. Fig. 8) is an important background, which mimics the signal.

As mentioned above, the jets in this background are less forward than the two forward jets in the signal, so that the forward jet cuts (14) can suppress this background.

However, further effective suppression is still needed. In the case of pure leptonic mode, this can be significantly suppressed by vetoing the central jets [15]. But in the semileptonic mode, the signal $W^{\pm} \to j_1 j_2$ is in the central rapidity region, so that central jet veto cannot be applied. Reference [21] considered the reconstruction of top quark, and eliminated this background by vetoing the events containing a top quark. Since we have already extracted the "single jet" J of $j_1 j_2$ satisfying the conditions (16) and (19), the momentum of the single jet can be measured. Then we can combine this single jet with the remaining jets j (the b jets) to reconstruct the top quark mass. Figure 9 depicts the invariant mass M_{Jj} distributions for the top quark background and the $pp \to W^+W^{\pm} j_1^f j_2^f$ process, which shows that we can extract the top quark peak by requiring [21]

$$130 \text{ GeV} < M_{Jj} < 240 \text{ GeV}. \tag{20}$$

We do it event by event, and veto the events containing the top quark. This *top quark veto* requirement can further suppress the top quark background. The effect of this veto is listed in the sixth row in Table I.

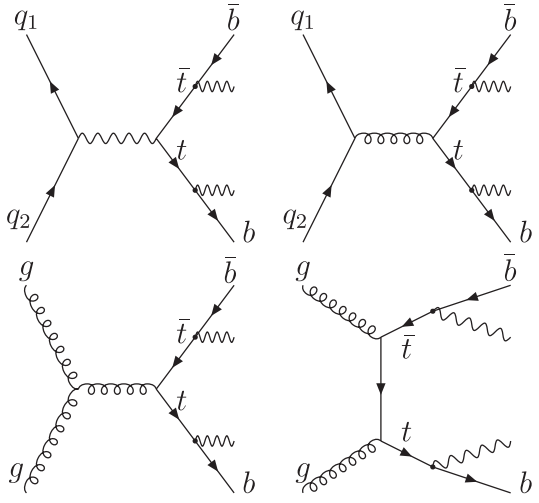

FIG. 8. Typical diagrams for the $t\bar{t}$ background $gg \to t\bar{t} \to bW^+\bar{b}W^-$.

D. Additional cuts

There are two commonly imposed additional cuts to suppress the backgrounds. The first one is the p_T *balance* requirement [23] (it is called *hard* p_T in Ref. [21]). Note that the signal process is a *hard process* in which the sum of the transverse momenta (p_T) of the final state particles vanishes (p_T balance). In the mentioned QCD backgrounds, there are undetected missing jets, which carry p_T, so that summing up the p_T of the detected final state particles will not vanish. Therefore, imposing the requirement of p_T balance can further suppress this kind of background. Considering the resolution of p_T measurement [22], we impose the following p_T balance requirement [23]:

$$\sum_i p_T^i < \pm 15 \text{ GeV}, \tag{21}$$

where p_T^i is the transverse momentum of the i-th final state particle.

Another additional cut commonly used is called *minijet veto*. For the signal process, there is no color exchange between the forward jet quarks and the $W^{\pm}$ decay jet J. However, color exchange is expected in the background processes due to the remnant-remnant interactions, which can produce minijets. Therefore, one can impose the additional cut of *minijet veto* by vetoing the events containing jets other than the signal jet J from $W^{\pm}$ decay [satisfying (15) and (16)] in the central rapidity region, $|\eta| < 2$ [21].

The efficiencies of these additional cuts are shown in the last two rows in Table I.

To illustrate the efficiencies of all these cuts, we list the cross sections (in fb) for the signal with irreducible background (IB), IB (obtained from the same process but with $f_W = 0$), the QCD backgrounds, and the top quark background in Table I for $m_H = 115$ GeV and $f_W/\Lambda^2 = 4$ TeV^{-2} (with other anomalous couplings vanishing) as an example. We see that the cuts can significantly suppress the backgrounds. Table I shows that *minijet veto* does not affect the results much because the above cuts have already very efficiently suppressed the backgrounds. After the cuts, the main remained background is the irreducible background, which is similar to the signal but is not enhanced at high energies by the momentum dependence of the anomalous couplings.

IV. NUMERICAL RESULTS

From (6) we see that the anomalous couplings $g^{(i)}_{HVV}$ ($i = 1, 2$, V stands for γ, $W^{\pm}$, Z^0) are related to four parameters, namely, f_W, f_{WW}, f_B, f_{BB}. For the process $pp \to W^+W^{\pm}j_1^f j_2^f$, except for the small contributions related to the photon, the main contributions are from the anomalous couplings of the Higgs boson to the weak gauge bosons, which is mainly contributed by f_W and f_{WW} since the contributions from f_B and f_{BB} are suppressed by a factor of $\sin^2\theta_W$ or $\sin^4\theta_W$ [cf. Equation (6)]. In the following, we only take account of the contributions related to f_W and f_{WW}, and neglect the f_B and f_{BB} contributions (setting f_B, $f_{BB} = 0$). With the above kinematic cuts, We give a full tree level calculation of the signal and background cross sections, event numbers, statistical significance [using Eq. (11)] for several values of integrated luminosity with various values of f_W/Λ^2 and f_{WW}/Λ^2 for $m_H = 115$, 160, and 200 GeV. In this paper, we only take into account the statistical uncertainty. The issue related to the systematic error is beyond the scope of this paper, and we leave it to the experimentalists.

For simplicity, we first make a one-parameter study, i.e., considering the cases of f_W/Λ^2 dominant and f_{WW}/Λ^2 dominant separately. We shall discuss the two-parameter study in the end of this section.

First, we list in Table II the obtained cross sections with various values of f_W/Λ^2 and f_{WW}/Λ^2 (in TeV^{-2}) for $m_H = 115$, 160, and 200 GeV. Note that the positive and negative regions of f_W/Λ^2 and f_{WW}/Λ^2 are not symmetric due to the interference between the signal and irreducible background amplitudes. We see that the cross sections are of the order of 1 fb, which are larger than those in the pure leptonic mode ($O(0.1$ fb)) [8] by and order of magnitude. The largeness of the cross sections is due to: (i) the branching ratio for $W \to j_1 j_2$ is larger than that for $W \to l^+\nu_l$, and (ii) we have included the process $pp \to W^+W^-j_1^f j_2^f \to l^+\nu_l j_1 j_2 j_1^f j_2^f$ as well, and with the improved cuts.

From Table II we see that for an integrated luminosity of 100 fb^{-1}, there can be of $O(10^2)$ events detected at the LHC. This not only reduces the statistical uncertainty relative to that in the pure leptonic mode, but also provides the possibility of measuring the differential cross sections. This is the advantage of the semileptonic mode.

Next, we take an integrated luminosity of $\mathcal{L}_{\rm int} \equiv \int dt\mathcal{L} = 100$ fb^{-1} to calculated the event numbers and using the approach of Eq. (11) to find out the sensitivities of f_W/Λ^2 and f_{WW}/Λ^2 (in TeV^{-2}) [and the related $g^{(i)}_{HVV}$ (in TeV^{-1}) in Eq. (6)] corresponding to the statistical significance of 1σ, 2σ and 3σ for $m_H = 115$, 160 and 200 GeV. The results are listed in Eqs. (22)–(24).

TABLE II. Cross sections (in fb) for $pp \to W^+W^{\pm}j_1^f j_2^f \to l^+\nu_l j_1 j_2 j_1^f j_2^f$ ($l^+ = e^+$, μ^+) at the LHC with various values of f_W/Λ^2 and f_{WW}/Λ^2 (in TeV^{-2}) for $m_H = 115$, 160, and 200 GeV.

m_H (GeV)	$\frac{f_W}{\Lambda^2}$ (TeV^{-2})								
	−4.0	−3.0	−2.0	−1.0	0	1.0	2.0	3.0	4.0
115	3.23	2.91	1.26	1.06	1.19	1.18	1.51	1.82	2.28
160	1.65	1.32	1.15	1.13	1.22	1.43	1.65	1.77	2.18
200	1.93	1.86	1.80	1.79	1.82	2.30	2.43	2.53	2.66
m_H (GeV)	$\frac{f_{WW}}{\Lambda^2}$ (TeV^{-2})								
	−4.0	−3.0	−2.0	−1.0	0	1.0	2.0	3.0	4.0
115	4.88	3.11	1.66	1.37	1.19	1.34	2.04	3.34	5.36
160	12.35	4.48	2.10	1.36	1.22	1.64	2.70	4.12	6.90
200	11.50	5.61	3.27	2.11	1.82	2.26	2.74	4.46	6.94

For $m_H = 115$ GeV and $\mathcal{L}_{\rm int} = 100$ fb^{-1} (f_W/Λ^2, f_{WW}/Λ^2 in TeV^{-2}, $g^{(i)}_{HVV}$ in TeV^{-1}), the results are

$$
\begin{aligned}
1\sigma:\ & -2.0 < f_W/\Lambda^2 < 1.2, \quad -0.4 < f_{WW}/\Lambda^2 < 0.8, \quad -0.053 < g^{(1)}_{HWW} < 0.032, \quad -0.042 < g^{(2)}_{HWW} < 0.021,\\
& -0.053 < g^{(1)}_{HZZ} < 0.032, \quad -0.016 < g^{(2)}_{HZZ} < 0.008, \quad -0.029 < g^{(1)}_{HZ\gamma} < 0.017,\\
& -0.018 < g^{(2)}_{HZ\gamma} < 0.009, \quad -0.005 < g_{H\gamma\gamma} < 0.002.\\
2\sigma:\ & -2.2 < f_W/\Lambda^2 < 1.6, \quad -1.1 < f_{WW}/\Lambda^2 < 1.1, \quad -0.058 < g^{(1)}_{HWW} < 0.042, \quad -0.058 < g^{(2)}_{HWW} < 0.058,\\
& -0.058 < g^{(1)}_{HZZ} < 0.042, \quad -0.022 < g^{(2)}_{HZZ} < 0.022, \quad -0.032 < g^{(1)}_{HZ\gamma} < 0.023,\\
& -0.024 < g^{(2)}_{HZ\gamma} < 0.024, \quad -0.007 < g_{H\gamma\gamma} < 0.007.\\
3\sigma:\ & -2.4 < f_W/\Lambda^2 < 1.9, \quad -1.5 < f_{WW}/\Lambda^2 < 1.3, \quad -0.063 < g^{(1)}_{HWW} < 0.050, \quad -0.068 < g^{(2)}_{HWW} < 0.079,\\
& -0.063 < g^{(1)}_{HZZ} < 0.050, \quad -0.026 < g^{(2)}_{HZZ} < 0.030, \quad -0.035 < g^{(1)}_{HZ\gamma} < 0.027,\\
& -0.029 < g^{(2)}_{HZ\gamma} < 0.033, \quad -0.008 < g_{H\gamma\gamma} < 0.009. \qquad (22)
\end{aligned}
$$

For $m_H = 160$ GeV and $\mathcal{L}_{\rm int} = 100$ fb^{-1} (f_W/Λ^2, f_{WW}/Λ^2 in TeV^{-2}, $g^{(i)}_{HVV}$ in TeV^{-1}), the results are

$$
\begin{aligned}
1\sigma:\ & -2.7 < f_W/\Lambda^2 < 0.3, \quad -0.9 < f_{WW}/\Lambda^2 < 0.2, \quad -0.071 < g^{(1)}_{HWW} < 0.008, \quad -0.011 < g^{(2)}_{HWW} < 0.047,\\
& -0.071 < g^{(1)}_{HZZ} < 0.008, \quad -0.004 < g^{(2)}_{HZZ} < 0.018, \quad -0.039 < g^{(1)}_{HZ\gamma} < 0.004,\\
& -0.004 < g^{(2)}_{HZ\gamma} < 0.020, \quad -0.001 < g_{H\gamma\gamma} < 0.005.\\
2\sigma:\ & -3.4 < f_W/\Lambda^2 < 0.9, \quad -1.1 < f_{WW}/\Lambda^2 < 0.5, \quad -0.089 < g^{(1)}_{HWW} < 0.024, \quad -0.026 < g^{(2)}_{HWW} < 0.058,\\
& -0.089 < g^{(1)}_{HZZ} < 0.024, \quad -0.010 < g^{(2)}_{HZZ} < 0.022, \quad -0.049 < g^{(1)}_{HZ\gamma} < 0.013,\\
& -0.011 < g^{(2)}_{HZ\gamma} < 0.024, \quad -0.003 < g_{H\gamma\gamma} < 0.007.\\
3\sigma:\ & -3.8 < f_W/\Lambda^2 < 1.5, \quad -1.3 < f_{WW}/\Lambda^2 < 0.8, \quad -0.100 < g^{(1)}_{HWW} < 0.039, \quad -0.042 < g^{(2)}_{HWW} < 0.068,\\
& -0.100 < g^{(1)}_{HZZ} < 0.039, \quad -0.016 < g^{(2)}_{HZZ} < 0.026, \quad -0.055 < g^{(1)}_{HZ\gamma} < 0.022,\\
& -0.018 < g^{(2)}_{HZ\gamma} < 0.029, \quad -0.005 < g_{H\gamma\gamma} < 0.008. \qquad (23)
\end{aligned}
$$

For $m_H = 200$ GeV and $\mathcal{L}_{\rm int} = 100$ fb^{-1} (f_W/Λ^2, f_{WW}/Λ^2 in TeV^{-2}, $g^{(i)}_{HVV}$ in TeV^{-1}), the results are

$$
\begin{aligned}
1\sigma:\ & -3.2 < f_W/\Lambda^2 < 0.2, \quad -0.7 < f_{WW}/\Lambda^2 < 0.2, \quad -0.084 < g^{(1)}_{HWW} < 0.005, \quad -0.011 < g^{(2)}_{HWW} < 0.037,\\
& -0.084 < g^{(1)}_{HZZ} < 0.005, \quad -0.004 < g^{(2)}_{HZZ} < 0.014, \quad -0.046 < g^{(1)}_{HZ\gamma} < 0.003,\\
& -0.004 < g^{(2)}_{HZ\gamma} < 0.015, \quad -0.001 < g_{H\gamma\gamma} < 0.004.\\
2\sigma:\ & -4.1 < f_W/\Lambda^2 < 0.6, \quad -1.0 < f_{WW}/\Lambda^2 < 0.7, \quad -0.108 < g^{(1)}_{HWW} < 0.016, \quad -0.037 < g^{(2)}_{HWW} < 0.053,\\
& -0.108 < g^{(1)}_{HZZ} < 0.016, \quad -0.014 < g^{(2)}_{HZZ} < 0.020, \quad -0.059 < g^{(1)}_{HZ\gamma} < 0.009,\\
& -0.015 < g^{(2)}_{HZ\gamma} < 0.022, \quad -0.004 < g_{H\gamma\gamma} < 0.006.\\
3\sigma:\ & -4.3 < f_W/\Lambda^2 < 0.8, \quad -1.2 < f_{WW}/\Lambda^2 < 1.0, \quad -0.113 < g^{(1)}_{HWW} < 0.021, \quad -0.053 < g^{(2)}_{HWW} < 0.063,\\
& -0.113 < g^{(1)}_{HZZ} < 0.021, \quad -0.020 < g^{(2)}_{HZZ} < 0.024, \quad -0.062 < g^{(1)}_{HZ\gamma} < 0.012,\\
& -0.022 < g^{(2)}_{HZ\gamma} < 0.027, \quad -0.006 < g_{H\gamma\gamma} < 0.007. \qquad (24)
\end{aligned}
$$

Equation (22) is to be compared with the sensitivities in the pure leptonic mode with $m_H = 115$ GeV for an integrated luminosity of 300 fb^{-1} (f_W/Λ^2 and f_{WW}/Λ^2 are in TeV^{-2}) [8].

$$
\begin{aligned}
&1\sigma\text{: } -1.0 < f_W/\Lambda^2 < 0.85, \quad -1.6 < f_{WW}/\Lambda^2, 1.6,\\
&2\sigma\text{: } -1.4 < f_W/\Lambda^2 < 1.2, \quad -2.2 < f_{WW}/\Lambda^2 < 2.2,\\
&3\sigma\text{: } -1.7 < f_W/\Lambda^2 < 1.6, \quad -2.9 < f_{WW}/\Lambda^2 < 2.9.
\end{aligned} \tag{25}
$$

Note that f_W/Λ^2 is more sensitive in the pure leptonic mode, while f_{WW}/Λ^2 is more sensitive in the semileptonic mode. This is because that the process considered in the pure leptonic mode is only $pp \to W^+W^+j_1^f j_2^f$, while it is $pp \to W^+W^\pm j_1^f j_2^f$ in the semileptonic mode. Anyway, the 2σ sensitivities in the two modes are of the same level. Since the required integrated luminosity in the pure leptonic mode is 300 fb^{-1}, while it is only 100 fb^{-1} in the semileptonic mode, the semileptonic mode can reduce the required integrated luminosity by a factor of 3 relative to the pure leptonic mode. So the anomalous couplings can be measured to this sensitivity when the LHC reaches its designed luminosity, 100 fb^{-1}/year, or even earlier. This is quite promising.

So far we have concentrated on the study of the detection sensitivities. In the real world, the actual anomalous coupling(s) might be larger than the sensitivity bound(s) given above. So nonvanishing anomalous coupling(s) might even be detected for lower integrated luminosities at the LHC. Let us take the integrated luminosity of 50 fb^{-1} as an example. In Table III, we list the numbers of events for $pp \to W^+W^\pm j_1^f j_2^f \to l^+\nu_l j_1 j_2 j_1^f j_2^f$ at the LHC for an integrated luminosity of 50 fb^{-1} with various values of f_W/Λ^2 and f_{WW}/Λ^2 (in TeV^{-2}) for $m_H = 115$, 160 and 200 GeV. The values of the statistical significance $\sigma_{\rm stat}$ are shown in the parentheses.

Our calculation shows that the sensitivity bounds for $m_H = 115$–200 GeV and $\mathcal{L}_{\rm int} = 50$ fb^{-1} are

$$
\begin{aligned}
&1\sigma\text{: } -3.5\ \text{TeV}^{-2} \le f_W/\Lambda^2 \le 1.3\ \text{TeV}^{-2},\\
&\quad -0.9\ \text{TeV}^{-2} \le f_{WW}/\Lambda^2 \le 0.8\ \text{TeV}^{-2},\\
&3\sigma\text{: } -4.5\ \text{TeV}^{-2} \le f_W/\Lambda^2 \le 2.4\ \text{TeV}^{-2},\\
&\quad -2.0\ \text{TeV}^{-2} \le f_{WW}/\Lambda^2 \le 1.5\ \text{TeV}^{-2}.
\end{aligned} \tag{26}
$$

If the anomalous coupling constants in the nature are beyond the 1σ bounds in (26), the LHC can already detect their effect with several tens to a hundred of events when the integrated luminosity reaches 50 fb^{-1}. This is quite promising since it can be started within the first couple of years run of the LHC. If they are beyond the 3σ bounds, the LHC can perform a 3σ detection for an integrated luminosity of 50 fb^{-1}. If the experiment does not find the evidence of the anomalous couplings at the LHC for an integrated luminosity of 50 fb^{-1}, it means that f_W/Λ^2 and f_{WW}/Λ^2 are within the 1σ sensitivity bounds given in (26), and further detection with higher integrated luminosity is needed.

Finally, we show some results of the two-parameter study.

As mentioned above, with the large cross sections in the semileptonic mode, we can study differential cross sections, which behave differently for different values of f_W and f_{WW}, so that we can determine f_W and f_{WW} separately from this information. As an example, we plot, in Fig. 10, the $p_T(l^+)$ distributions for $m_H = 115$ GeV and $\mathcal{L}_{\rm int} = 100$ fb^{-1} contributed by three different sets of f_W/Λ^2 and f_{WW}/Λ^2 from different regions in the two-parameter space, namely, the cases of $f_W/\Lambda^2 = 2$ TeV$^{-2} \gg f_{WW}/\Lambda^2$, $f_{WW}/\Lambda^2 = 2$ TeV$^{-2} \gg f_W/\Lambda^2$, and $f_W/\Lambda^2 = -f_{WW}/\Lambda^2 = 2$ TeV^{-2}. We see that the three $p_T(l^+)$ distributions are different and quite distinguishable especially in the region near 200 GeV. Since the cross section is more sensitive to f_{WW}/Λ^2 than to f_W/Λ^2, the curve of the $f_{WW}/\Lambda^2 = 2$ TeV$^{-2} \gg f_W/\Lambda^2$ case lies significantly higher than that of the $f_W/\Lambda^2 = 2$ TeV$^{-2} \gg f_{WW}/\Lambda^2$ case. From Eq. (6) we see that f_W/Λ^2 appears in the formulae always with a positive sign, while f_{WW}/Λ^2 appears always with a negative sign. So that in the case of $f_W/\Lambda^2 = -f_{WW}/\Lambda^2 = 2$ TeV^{-2}, these two contributions are constructive, and thus this curve lies well above the two former curves. Therefore, measuring both the cross section and the $p_T(l^+)$ distribution may help to separately determine the two parameters f_W and f_{WW} to a certain precision. If there is no characteristic signal for new physics

TABLE III. Numbers of events for $pp \to W^+W^\pm j_1^f j_2^f \to l^+\nu_l j_1 j_2 j_1^f j_2^f$ ($l^+ = e^+$, μ^+) at the LHC for an integrated luminosity of 50 fb^{-1} with various values of f_W/Λ^2 and f_{WW}/Λ^2 (in TeV^{-2}) for $m_H = 115$, 160 and 200 GeV. The values of the statistical significance $\sigma_{\rm stat}$ are shown in the parentheses.

m_H (GeV)	$\frac{f_W}{\Lambda^2}$ (TeV^{-2})								
	−4.0	−3.0	−2.0	−1.0	0	1.0	2.0	3.0	4.0
115	162 (13.21)	146 (11.16)	63 (0.81)	53 (−)	60 (0)	59 (−)	76 (2.12)	91 (4.05)	114 (7.09)
160	83 (2.75)	66 (1.09)	58 (−)	57 (−)	61 (0)	72 (1.58)	83 (2.75)	89 (3.50)	109(6.09)
200	96 (1.01)	93 (0.79)	90 (−)	89 (−)	91 (0)	115 (2.54)	121 (3.18)	126 (3.71)	133 (4.39)
m_H (GeV)	$\frac{f_{WW}}{\Lambda^2}$ (TeV^{-2})								
	−4.0	−3.0	−2.0	−1.0	0	1.0	2.0	3.0	4.0
115	244 (23.89)	156 (12.41)	83 (3.06)	69 (1.39)	60 (0)	67 (1.28)	102 (5.51)	167 (13.91)	268 (26.99)
160	618 (71.13)	224 (20.85)	105 (5.61)	68 (1.18)	62 (0)	82 (2.75)	135 (9.42)	206 (18.52)	345 (36.30)
200	575 (50.14)	281 (19.56)	164 (7.39)	106 (1.56)	93 (0)	113 (2.17)	137 (4.64)	223 (13.56)	347 (26.44)

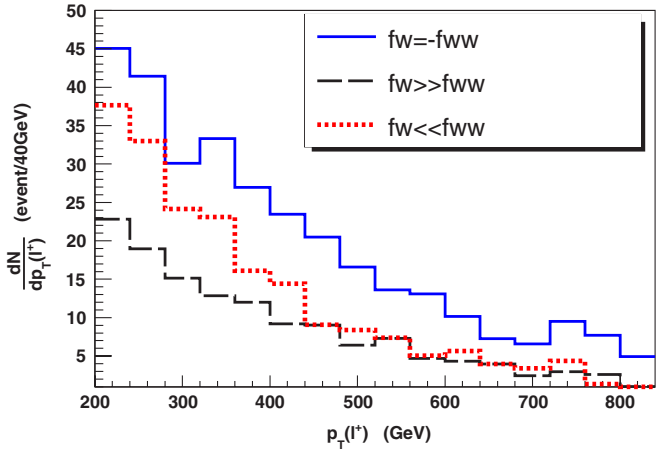

FIG. 10 (color online). Lepton transverse momentum distributions in the case of $m_H = 115$ GeV for an integrated luminosity of 100 fb^{-1} taking the cases of $f_W/\Lambda^2 = 2$ TeV$^{-2} \gg f_{WW}/\Lambda^2$, $f_{WW}/\Lambda^2 = 2$ TeV$^{-2} \gg f_W/\Lambda^2$ and $f_W/\Lambda^2 = -f_{WW}/\Lambda^2 = 2$ TeV^{-2} as examples.

model found before this measurement, the values of f_W and f_{WW} may serve as a clue for probing the underlying theory of new physics. This is an advantage of the semileptonic mode over the pure leptonic mode.

V. CONCLUSION

In this paper, we have given a full tree level study of the test of anomalous gauge couplings [cf. Eqs. (1) and (6)] at the LHC via the WW scattering processes $pp \to W^+W^+j_1^f j_2^f$ and $pp \to W^+W^-j_1^f j_2^f$ in the semileptonic mode $W^+ \to l^+\nu_l$, $W^+(W^-) \to j_1 j_2$. Through out this paper, we take into account only the statistical uncertainty. The issue of systematic error is beyond the scope of this paper, and we leave it to the experimentalists.

Both signals and backgrounds are calculated at the hadron level with suitably imposed kinematic cuts to suppress the backgrounds. As we mentioned in Sec. III A, the signal and irreducible background should to calculated together to guarantee gauge invariance. The efficiencies of the cuts are shown in Table I, which shows that the cuts [13–21] can suppress the QCD backgrounds and the $t\bar{t}$ background quite efficiently. After the cuts, the main background remained is the irreducible background.

The obtained cross sections for $m_H = 115$, 160, and 200 GeV in the ranges $|f_W/\Lambda^2| \le 4$ and $|f_{WW}/\Lambda^2| \le 4$ are listed in Table II. Because of the largeness of the branching ratio $B(W^\pm \to j_1 j_2)$, the contributions of both $pp \to W^+W^+j_1^f j_2^f$ and $pp \to W^+W^-j_1^f j_2^f$, and the improved cuts, the cross sections are as large as of $O(1$ fb$) - O(10$ fb$)$. So that for an integrated luminosity of 100 fb^{-1}, hundreds of events can be detected at the LHC.

As mentioned in Sec. IV that the $pp \to W^+W^\pm j_1^f j_2^f$ processes are mainly sensitive to two anomalous coupling constants, f_W/Λ^2 and f_{WW}/Λ^2. We first made a one-parameter study, i.e., considering the cases of f_W/Λ^2 dominant and f_{WW}/Λ^2 dominant separately. Taking the integrated luminosity of 100 fb^{-1} as an example, the obtained results of the sensitivity ranges of f_W/Λ^2, f_{WW}/Λ^2 and the corresponding $g_{HVV}^{(i)}$'s for 1σ, 2σ and 3σ detections are listed in Eqs. (22) to (24) for $m_H = 115$ GeV, 160 GeV and 200 GeV. These are of the same level as those in the pure leptonic mode for an integrated luminosity of 300 fb^{-1}. Thus, for the same level of sensitivity, the semileptonic mode can reduce the required integrated luminosity by a factor of 3.

If the actual anomalous coupling constants in nature are not so small, it can even be measured with a low luminosity as 50 fb^{-1}. The obtained event numbers and statistical significance $\sigma_{\rm stat}$ for an luminosity of 50 fb^{-1} are listed in Table III, which shows that a detection with around $O(100)$ events can be performed at the LHC for an integrated luminosity of 50 fb^{-1} if the anomalous coupling constants in the nature are larger than the 1σ bounds given in Eq. (26). This can be done within the first couple of years run of the LHC. So it is quite promising. If the detected result is consistent with the SM value at the LHC for an integrated luminosity of 50 fb^{-1}, it means that f_W/Λ^2 and f_{WW}/Λ^2 are within the 1σ sensitivity bounds (26), and further detection with higher integrated luminosity is needed.

We have also made a simple two-parameter study considering f_W/Λ^2 and f_{WW}/Λ^2 simultaneously. With the hundreds of events for $\mathcal{L}_{\rm int} = 100$ fb^{-1}, it is possible to measure the p_T distribution of the charged lepton experimentally. We plotted in Fig. 10 the $p_T(l^+)$ distributions for $m_H = 115$ GeV and $\mathcal{L}_{\rm int} = 100$ fb^{-1} corresponding to $f_W/\Lambda^2 = 2$ TeV$^{-2} \gg f_{WW}/\Lambda^2$, $f_{WW}/\Lambda^2 = 2$ TeV$^{-2} \gg f_W/\Lambda^2$, and $f_W/\Lambda^2 = -f_{WW}/\Lambda^2 = 2$ TeV^{-2} as examples. It shows that the three distributions are quite distinguishable. Therefore, measuring both the total cross section and the $p_T(l^+)$ distribution may determine the two parameters f_W/Λ^2 and f_{WW}/Λ^2 separately to certain precision. This may provide a clue for figuring out the underlying theory of new physics beyond the SM if no other characteristic signal of the new physics is found before that measurement.

In summary, the process $pp \to W^+W^\pm j_1^f j_2^f \to l^+\nu_l j_1 j_2 j_1^f j_2^f$ at the LHC can provide a sensitive test of the anomalous gauge couplings of the Higgs boson showing the effect of new physics beyond the SM. The experiment can start the test for an integrated luminosity around 50 fb^{-1}, and can measure the total cross section and the p_T distributions of the charged lepton to certain precision for an integrated luminosity of 100 fb^{-1}. With such measurements, it is possible to determine the two main parameters f_W/Λ^2 and f_{WW}/Λ^2 of the anomalous couplings separately, which may provide a clue for figuring out the underlying theory of new physics.

ACKNOWLEDGMENTS

We would like to thank Y. Gao for useful discussions. This work is supported by National Natural Science Foundation of China under Grant Nos. 10635030, 10875064, 10705017, and 10435040.

[1] C. Amsler *et al.* (Particle Data Group), Phys. Lett. B **667**, 1 (2008).
[2] R. Dashen and H. Neuberger, Phys. Rev. Lett. **50**, 1897 (1983).
[3] L. Susskind, Phys. Rev. D **20**, 2619 (1979).
[4] K. Hagiwara, S. Ishihara, R. Szalapski, and D. Zeppenfeld, Phys. Rev. D **48**, 2182 (1993).
[5] W. Buchmüller and D. Wyler, Nucl. Phys. **B268**, 621 (1986); C. J. C. Burgess and H. J. Schnitzer, Nucl. Phys. **B228**, 464 (1983); C. N. Leung, S. T. Love, and S. Rao, Z. Phys. C **31**, 433 (1986).
[6] For a review, see M. C. Gonzalez-Garcia, Int. J. Mod. Phys. A **14**, 3121 (1999).
[7] R. Sekhar Chivukula and V. Koulovassilopouplos, Phys. Lett. B **309**, 371 (1993).
[8] Bin Zhang, Yu-Ping Kuang, Hong-Jian He, and C.-P. Yuan, Phys. Rev. D **67**, 114024 (2003).
[9] V. Barger, T. Han, P. Langacker, B. McEltrath, and P. M. Zerwas, Phys. Rev. D **67**, 115001 (2003).
[10] G. J. Gounaris, J. Layssac, and F. M. Renard, Phys. Lett. B **332**, 146 (1994); G. J. Gounaris, J. Layssac, J. E. Pascalis, and F. M. Renard, Z. Phys. C **66**, 619 (1995).
[11] O. J. P. Éboli, M. C. Gonzalez-Garcia, S. M. Lietti, and S. F. Novaes, Phys. Lett. B **478**, 199 (2000); F. de Campos, M. C. Gonzalez-Garcia, S. M. Lietti, S. F. Novaes, and R. Rosenfeld, Phys. Lett. B **435**, 407 (1998).
[12] T. Plehn, D. Rainwater, and D. Zeppenfeld, Phys. Rev. Lett. **88**, 051801 (2002).
[13] V. Barger, K. Cheung, A. Djouadi, B. A. Kniel, and P. M. Zerwas, Phys. Rev. D **49**, 79 (1994); M. Kramer, J. Kuhn, M. L. Stong, and P. M. Zerwas, Z. Phys. C **64**, 21 (1994); K. Hagiwara and M. Stong, Z. Phys. C **62**, 99 (1994); J. F. Gunion, T. Han, and R. Sobey, Phys. Lett. B **429**, 79 (1998); K. Hagiwara, S. Ishihara, J. Kamoshita, and B. A. Kniel, Eur. Phys. J. C **14**, 457 (2000).
[14] T. Han, Y.-P. Kuang, and B. Zhang, Phys. Rev. D **73**, 055010 (2006).
[15] J. Bagger, V. Barger, K. Cheung, J. Gunion, T. Han, G. A. Ladinsky, R. Rosenfeld, and C.-P. Yuan, Phys. Rev. D **49**, 1246 (1994); **52**, 3878 (1995).
[16] K. Hagiwara and D. Zeppenfeld, Nucl. Phys. **B313**, 560 (1989); V. Barger, T. Han, and D. Zeppenfeld, Phys. Rev. D **41**, 2782 (1990).
[17] T. Sjöstrand, P. Eden, C. Friberg, L. Lönnblad, G. Miu, S. Mrenna, and E. Norrbin, Comput. Phys. Commun. **135**, 238 (2001).
[18] J. Pumplin, D. R. Stump, J. Huston, H. L. Lai, P. Nadolsky, and W. K. Tung, J. High Energy Phys. 07 (2002) 012.
[19] S. Cantani *et al.*, Nucl. Phys. **B406**, 187 (1993).
[20] M. H. Seymour, Z. Phys. C **62**, 127 (1994).
[21] J. M. Butterworth, B. E. Cox, and J. R. Forshaw, Phys. Rev. D **65**, 096014 (2002).
[22] ATLAS Physics TDR, CERN Report No. CERN/LHCC/99-15, Vol. 1.
[23] H.-J. He, Y.-P. Kuang, Y.-H. Qi, B. Zhang, A. Belyaev, R. S. Chivukula, N. D. Christensen, A. Pukhov, and E. H. Simmons, Phys. Rev. D **78**, 031701(R) (2008).